Supplementary Information (SI) for Energy & Environmental Science.
This journal is © The Royal Society of Chemistry 2025

A 1.6 mW/cm^2 Lactate/O_2 Enzymatic Biofuel Cell: Enhanced Power Generation and Energy Harvesting from Human Sweat by 3D Interpenetrating Network Porous Structure CNT-Membranes

Hao Liu[1,2], Yang Lu[1], Andrew Xiang[5], Weili Zhang[1,2], Wenmin Kuang[4], Shuaishuai Yan[1], Qingbin Cao[1], Pan Zhou[1], Wenhui Hou[1], Fengxiang Liu[1], Haiyu Zhou[1], Xuan Song[1], Zhenjun Luo[2], Baichong Chao[2], Yong Xiang[3,*], Kai Liu[1,*]

[1]Department of Chemical Engineering, Tsinghua University, 100084, Beijing, China

[2]Hefei institute for Public Safety Research, Tsinghua University, 230031, Hefei, China

[3]University of Electronic Science and Technology of China, 611731, Chengdu, China

[4]Department of Engineering Physics, Tsinghua University, 100084, Beijing, China

[5]College of Letters and Science, University of California, Berkeley, CA 94704, USA

***Correspondence:** xiang@uestc.edu.cn; liukai2019@tsinghua.edu.cn

1. Materials and methods

1.1 Materials. The multiwalled carbon nanotubes (MWCNT) was procured from XFNANO (China). The Lactate oxidase (LOx, EC 1.13.12.4, 50U mg^{-1}) was obtained from AsahiKASEI. SEBS triblock copolymer, toluene, sodium bicarbonate ($NaHCO_3$), ethanol, hydrochloric acid (HCl), Tween-20, 1,4-naphthoquinone (NQ), chitosan, glutaraldehyde, acetic acid, Nafion perfluorinated resin solution (5%), acetone, bovine serum albumin (BSA), PBS simulated body fluid, L-lactate, platinum-carbon catalyst, buckypaper and hydrophobic carbon cloth were all purchased from Sigma Aldrich. Ultra-pure deionized water was used to prepare all the reagents and electrolytes.

1.2 CNT-membrane preparation. The CNT-membrane was synthesized by non-solvent induced phase separation (NIPS) technology using multiwalled carbon nanotubes (MWCNT) as membrane-matrix materials and styrene-ethyl butylene-styrene block copolymer (SEBS) as the elastomeric binder. As illustrated in Figure S1, 0.5g of SEBS was dissolved into a 18 mL toluene, and a certain quality of MWCNT, which was grinded with sodium bicarbonate ($NaHCO_3$) to disperse it evenly, was added to the above solution with continuing stirring for 6 hours to form a casting solution. In this context, SEBS and MWCNT were adjusted based on their mass ratio. After that, the CNT-membrane was obtained by casting the solution on clean glass plate using a membrane applicator with thickness of 1000 μm, and then promptly placed in an ethylalcohol coagulation bath at 20 °C for 60 min. And the wet CNT-membrane was taken out from the alcohol after the phase separation

process completed and make it dry naturally with the volatilization of alcohol. In order to remove $NaHCO_3$, the dry CNT-membrane was soaked in 0.5M hydrochloric acid solution for 12 hours to fully react. Finally, the CNT-membrane was obtained after washed with distilled water and dried at 80 ℃. The CNT-membrane not only exhibited abundant porous structure due to the dual diffusion between the solvent and the non-solvent but also presented excellent flexibility brought from the intertwining of CNTs and the viscoelasticity of SEBS. If the CNT-membrane was intended to be supported on hierarchical porous nickel, the glass substrate was replaced with a hierarchical porous nickel substrate, resulting in an integrated composite electrode of the CNT-membrane and nickel. The remaining procedures were identical to those described above.

1.3 CNT-Bioanode fabrication. The CNT-membrane was cut into 1 cm × 1 cm pieces and immersed in 1 wt% Tween-20 solution for 5 min. And the CNT-bioanode was fabricated as follows: Firstly, 10 μL of 0.2 M 1,4-NQ (dissolved in 9:1 vol/vol ethanol/acetone) was drop casted onto the CNT-membrane surface, followed by the addition 100 μL of LOx solution (40 mg mL^{-1} dissolved in 10 mg mL^{-1} of BSA). For immobilizing the enzyme, 10 μL of 1% glutaraldehyde solution and 1% chitosan (dissolved in 0.1 M acetic acid) were drop casted on the anode then kept at 4°C overnight. Each step was performed when the anode from the previous step had completely dried.

1.4 Air-cathode preparation. The air-cathode was fabricated using platinum/carbon (Pt/C, the platinum content is 20% or 40%) as catalyst supported hydrophobic

carbon cloth substrate. Before using, the hydrophobic carbon cloth was washed in alcohol for half an hour with ultrasonic and then dried at 80°C. The catalyst slurry was prepared using 20mg Pt/C catalyst dispersed in 500μL ethanol and 1000μL deionized water. To further enhance the mass transfer of O_2 on air-cathode, 500μL 5% (wt) Nafion solution was added in the slurry.

1.5 Electrode measurements. The microstructure and elementary distribution of CNT-membrane and air-cathode were measured by scanning electron microscopy (SEM, Zeiss Merlin) and additional energy dispersive spectroscopy (EDS). The distribution of LOx was observed by laser scanning confocal microscope (LSCM, A1HD25, Nikon Corporation of Japan). The porous structure parameters of CNT-membrane were assessed by the N_2 adsorption-desorption isotherm at 77 K using automatic adsorption system (BELSORP-max, Japan), while the pore size distribution was obtained by density functional theory (DFT) model. The flexibility and mechanical strength were tested by the tensile strength testing machine (HZ-1004, China). The electrical measurements were accomplished on a PARSTAT MC electrochemical workstation (Princeton, U.S.A.). Test area was a 1 cm × 1cm square in the middle of the CNT-membrane, using four-point probe method. By electrochemical impedance spectroscopy, the resistance of the membrane under different conditions can be read. Resistivity and conductivity can further be conducted. The mechanical strength was performed by electronic universal material testing machine. The water contact angle was measured using optical contact angle measuring device (OCA15EC Dataphysics GMBH). An electrochemical

workstation (CHI760e, Shanghai Chenhua Instrument Co., China) was used to obtain electrochemical data. For traditional three-electrode system, the modified electrode, Ag/AgCl electrode (saturated by KCl) and Pt net were applied as working, reference and counter electrodes, respectively. The cyclic voltammetry (CV) was operated at the scan rate of 10 mV s^{-1} from −0.2 V to 0.6 V in artificial sweat at room temperature. The polarization curves were performed at the potential vs Ag/AgCl from −0.2 V to 0.6 V.

1.6 Electrochemical testing of BFC Devices. The enzyme biofuel cells (BFC) were assembled using CNT-boanode as anode, air-cathode as cathode and artificial sweat as electrolyte. The open circuit voltage of the BFC is measured using CHI760e, and the polarization curve is obtained by scanning from the open circuit voltage to 0V at a scanning speed of 5mV/s. The power density is then calculated based on the resulting polarization curve. The energy density was measured by continuous discharge of BFC at 0.1mA through the multichannel Battery Test System (Wuhan Land Electronic Co., Ltd). The self-power performance of HSBFC is obtained by monitoring the current curve of the battery in real time at a voltage of 0.6V at PARSTAT MC electrochemical workstation (Princeton, U.S.A.).

1.7 Construction of the HSBFC Module. The three module circuit patterns of HSBFC were designed with AutoCAD 2020 (Autodesk). Utilizing laser cutting technology, the PI film was precisely cut into a design pattern created in AutoCAD software. The third module employed a PI substrate coated with a conductive copper layer as the cutting target. Following the determination of the anticipated

size and structure of the copper layer, selective removal of any remaining copper was carried out under acidic conditions. The CNT-bioanode and air-cathode were precisely cut to the required shape, affixed to their corresponding positions, and bonded between layers using adhesive on the PI surface. Finally, the external circuit was connected to both the positive and negative poles via a Cu wire.

1.8 Fabrication of customized Bluetooth device and pulse sensor. To demonstrate the practicality of the proposed BFC can power a high-power microelectronic device in application, a custom circuit board featuring an MS50FSA Bluetooth Low Energy (BLE) radio and an STM32L071 CPU system was developed with a pulse sensor. The pulse sensor was purchased from Tsingsensor Technology Co., LTD (China). Due to the limited OCP of BFCs, which can hardly reach 1 V, it fails to meet the requirements of conventional electronic devices. Therefore, apart from supplying power for BLE and CPU, a BQ25504 boost converter is also equipped on the board to elevate the voltage level of BFC. The core circuit used for energy extraction from BFC relies heavily on this boost converter. The BQ25504 output is connected to a 1F capacitor, which charges up to 3.3V before triggering the analog switch off and connecting the charged capacitor to the rest of the circuit and power supply system. The sensor's response was then recorded by the CPU and transmitted via Bluetooth module for broadcast, all powered under boost. To enable measurement data to be captured via a custom-designed electronic device and wirelessly transferred to an included smartphone app for capture and visualization, we developed a special app. The initial programming of the app for the electronic

device was done using android studio, a software development kit that provided an integrated development environment for Bluetooth-based data visualization. Upon completion of development, the app would be installed on the smartphone, rendering it ready for integration with the sensor array. Subsequently, the sensor-monitored data was wirelessly transmitted via Bluetooth to the APP and instantaneously converted into a visual electrocardiograph.

1.9 Real-time electrocardiogram data measurement. The pulse sensor utilizes laser wavelengths to detect the internal blood vessels of the human fingertip, which subsequently indicates the heart's pulse. Therefore, when pressure is applied to the sensor by pinching a finger, it converts data from the finger's blood vessels into digital information via its CPU and transmits it through Bluetooth to a smartphone app for visualization. The human skin contact tests using HSBFC and the sensor were performed by the first author himself.

1.10 Numerical Simulation Using COMSOL Multiphysics. A three-dimensional multiphysics coupling model was developed based on the finite element method (FEM), and solved using the commercial software package COMSOL Multiphysics. The simulation results provided a comprehensive understanding of the mass transport dynamics of lactate molecules within the hierarchical porous structure of the bioelectrode. The model incorporated mass conservation, charge and current conservation, and electrochemical reaction kinetics, as detailed in the supplementary information. The relative error tolerance was set to 1.0×10^{-6}. The computational regions only involve a porous CNT-bioanode membrane with

different pore structures (shown in Fig.1a and Fig. S2d). During the finite element method, several simplified assumptions were applied to the model based on approaches developed in the literatures[1]: (1) The electrolyte was treated as a concentrate-solution. (2) The temperature effect was not taken into account. (3) Properties of the CNT-bioanodes and the sweat were assumed to be isotropic and homogeneous. (4) None of the side reactions was considered.

A set of equation about matter transfer physical fields have been employed for the diffusion process of lactate in the CNT-bioanode:

$$\frac{\partial C_i}{\partial t} + \nabla J_i + \mu \cdot \nabla C_i = R_i \quad \text{(S1)}$$

$$J_i = -D_i \nabla C_i - Z_i \mu_{mi} F C_i \nabla v \quad \text{(S2)}$$

Where C_i was the concentration of lactate, J_i was the total flux of sweat, μ was the velocity of sweat, t was the diffusion time, R_i was the amount of lactate on the CNT-bioanode, D_i was the diffusion coefficient of lactate, Z_i was charge number, μ_{mi} was the ionic mobility of sweat, F was Faraday constant, V was the electric potential.

1. Z. Lv, M. Yue, M. Ling, H. Zhang, J. Yan, Q. Zheng, X. Li, Adv. Energy Mater., 2021, 11, 202003725.

2 Charts and instructions

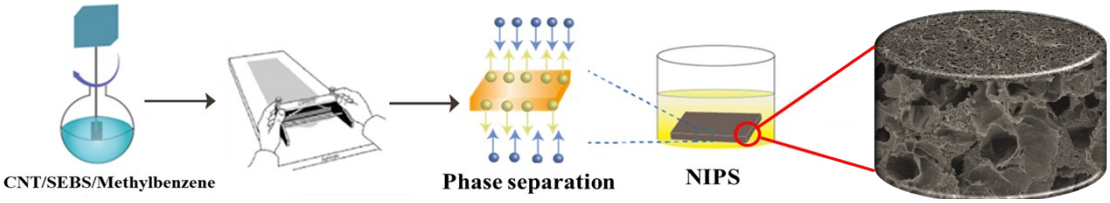

Figure S1 The preparation of CNT-membrane by NIPS.

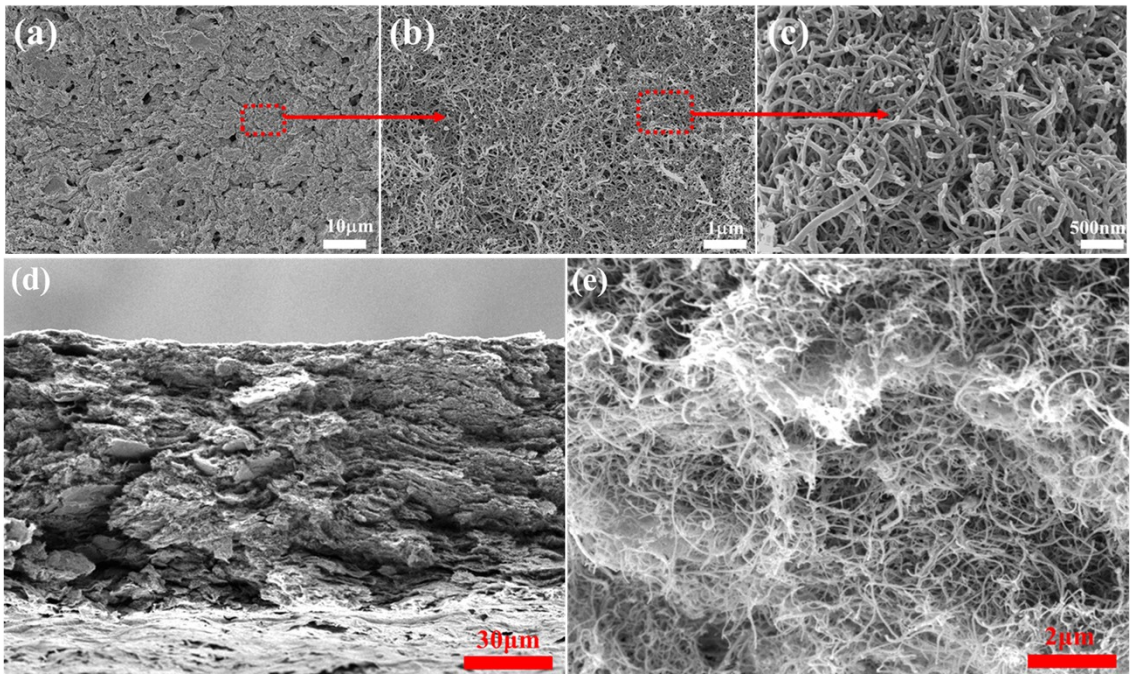

Figure S2 The surface structure of CNT-membrane (a-c) and images of the CNT-membrane after the pore structure has been removed by extensive mechanically rolling three times (d-e).

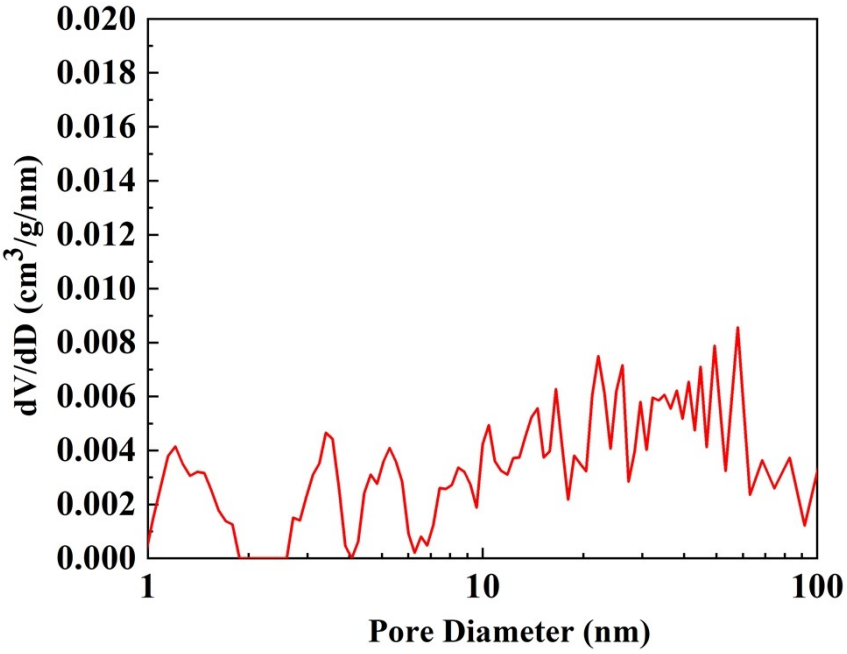

Figure S3 The pore size distribution of CNT-membrane.

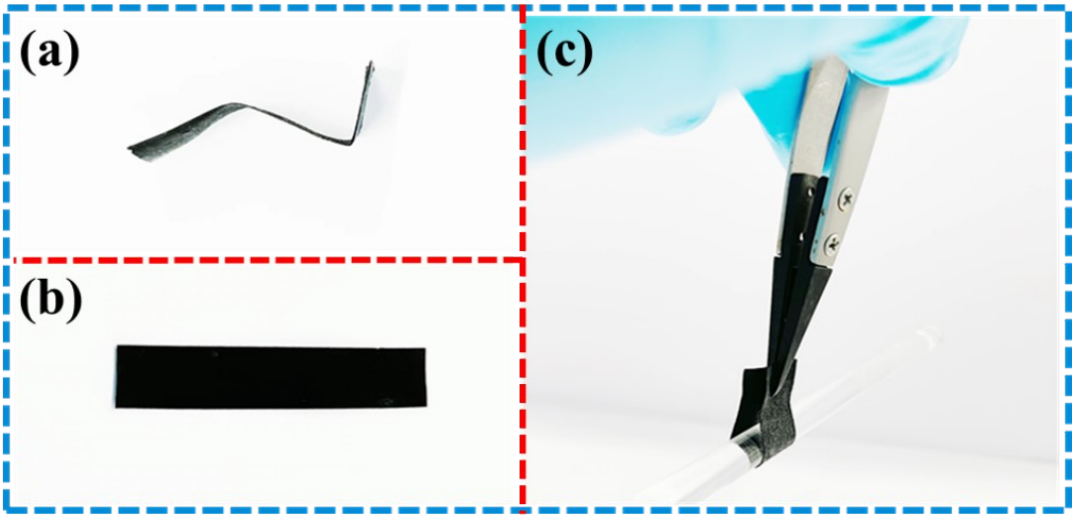

Figure S4 The optical photographs of flexibility and mechanical strength of CNT-membrane.

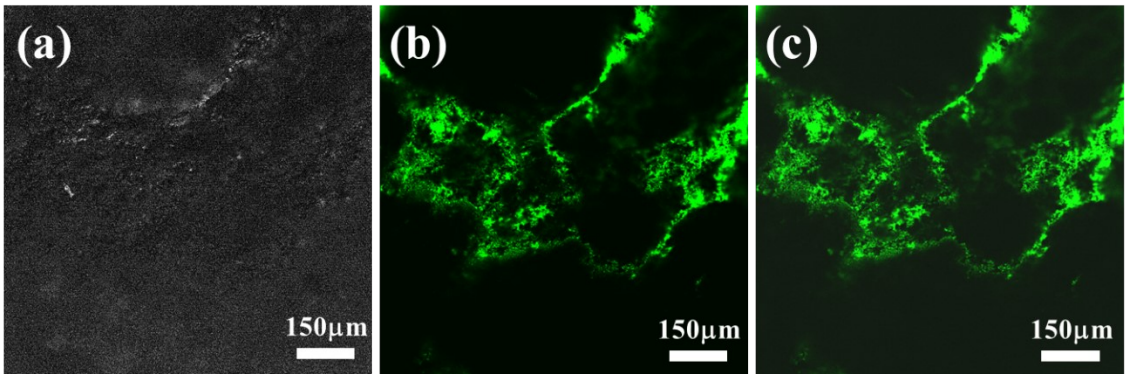

Figure S5 The GLSM of hydrophobic CNT-membrane loaded with LOx.

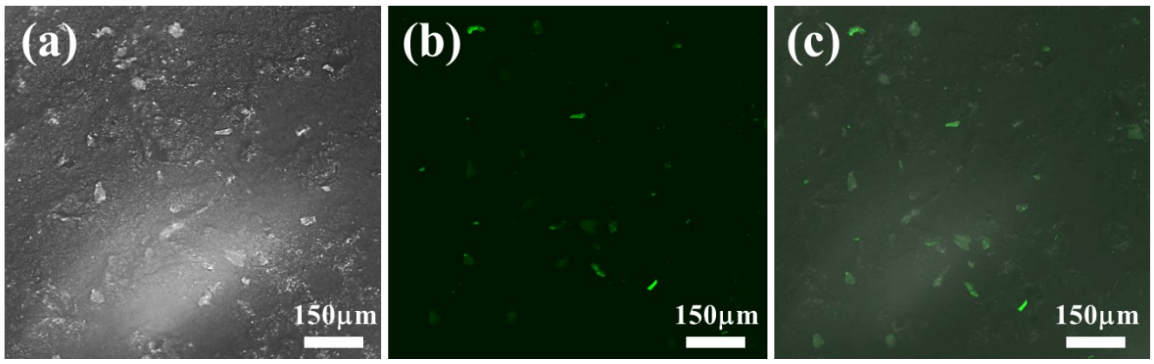

Figure S6 The GLSM of hydrophilic CNT-membrane devoid of LOx loading.

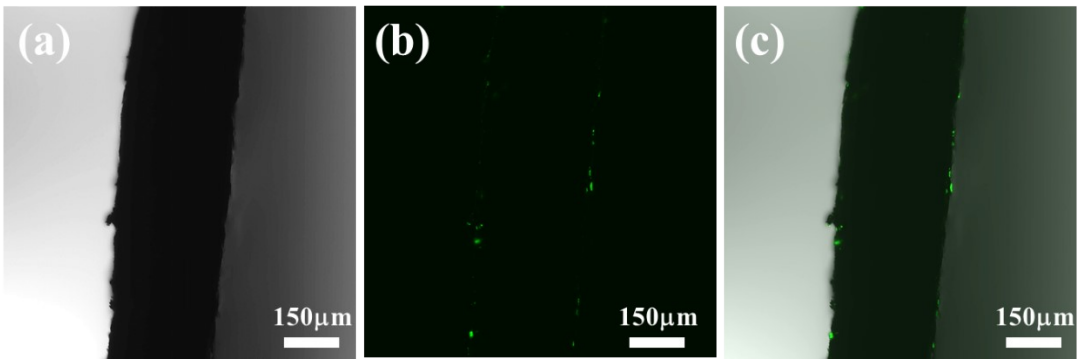

Figure S7 The GLSM of cross section of hydrophobic CNT-membrane loaded with LOx.

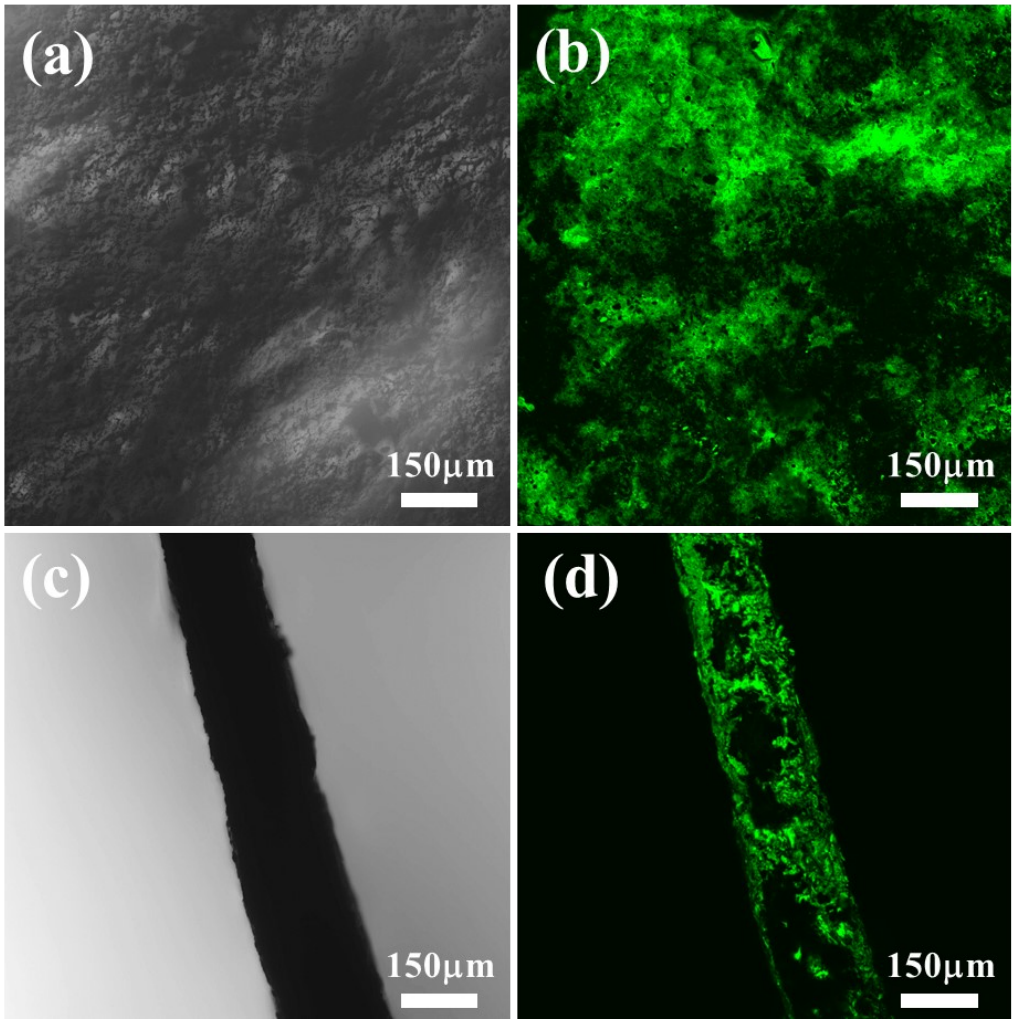

Figure S8 The GLSM of hydrophilic CNT-membrane with LOx loading.

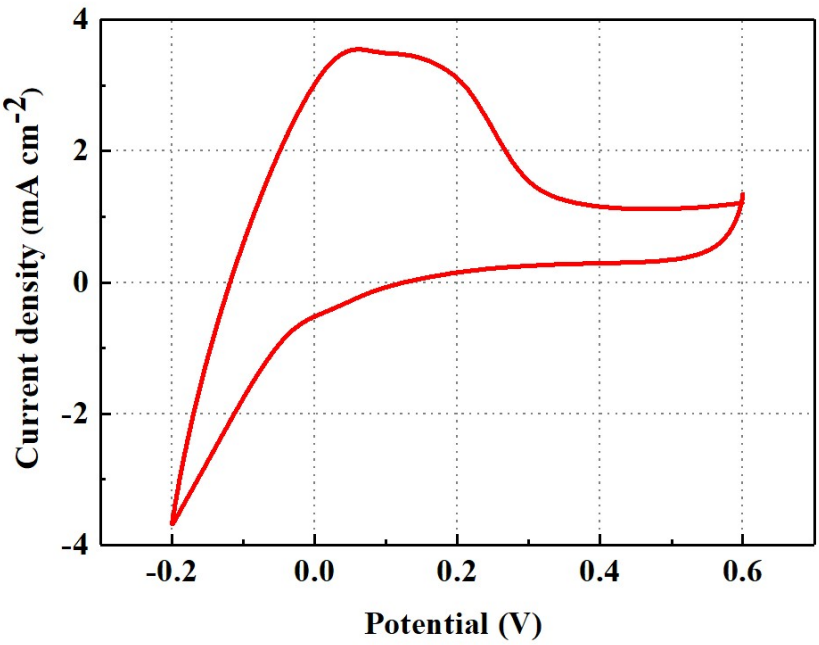

Figure S9 The CV curve of CNT-bioanode after eliminating its pore structure.

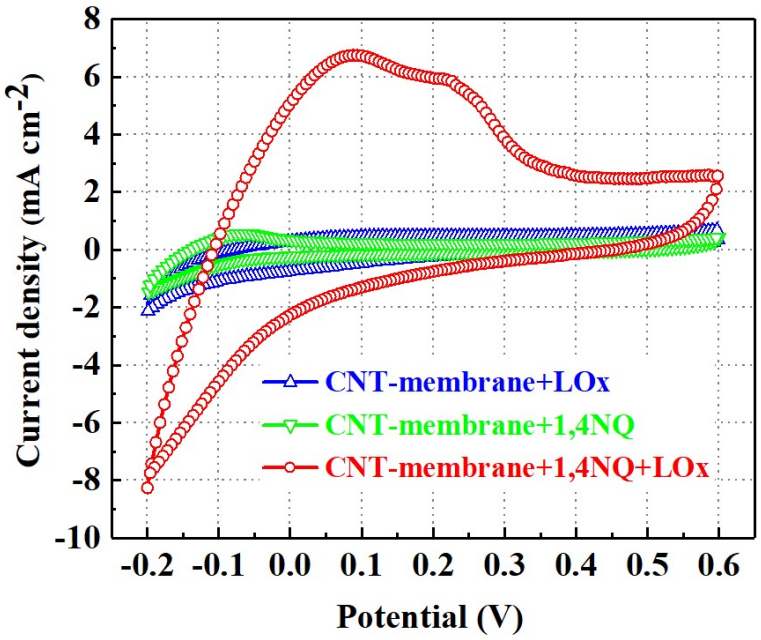

Figure S10 The CV curves of CNT-anode with or without LOx and 1,4-NQ.

Supplementary Note 1

The active site of LOx was coated with a protein layer approximately 5 nm thick. The isolated proteins encounter difficulty in electron exportation from the catalytic active site to the current collector, i. e. CNT-membrane. Thus, 1,4-NQ was utilized as a conductive mediator between LOx and CNT-membrane to address these issues. Based on the results of CV curves shown in Figure S10, it can be inferred that there was a high impedance between LOx and CNT-membrane when LOx was directly loaded onto the CNT-membrane, as evidenced by the absence of any discernible oxidation peak. In contrast, the utilization of 1,4-NQ as a conductive mediator resulted in an evident oxidation peak. However, the improvement in electrochemical properties of CNT-membrane loaded solely with 1,4-NQ was almost negligible. Thus, the conductive mediator is an essential requirement for CNT-membrane and LOx.

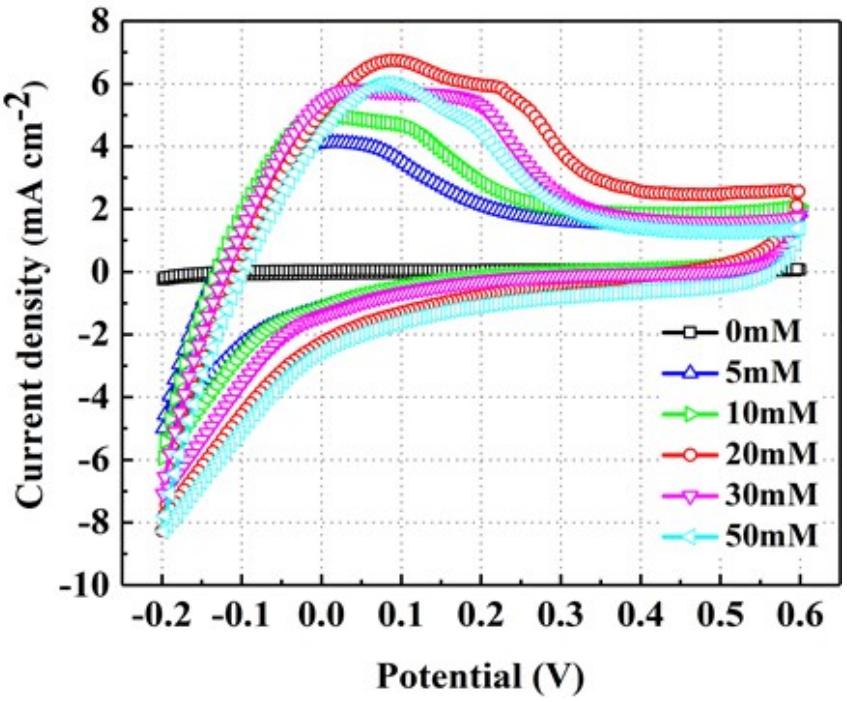

Figure S11 The CV curves of CNT-bioanode at different lactic acid concentrations.

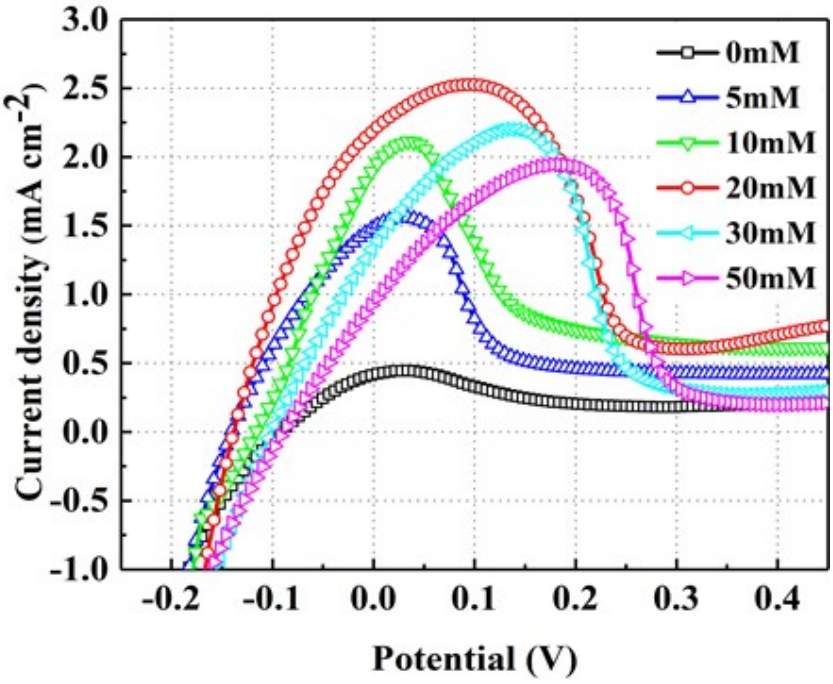

Figure S12 The LSV curves of CNT-bioanode at different lactic acid concentrations.

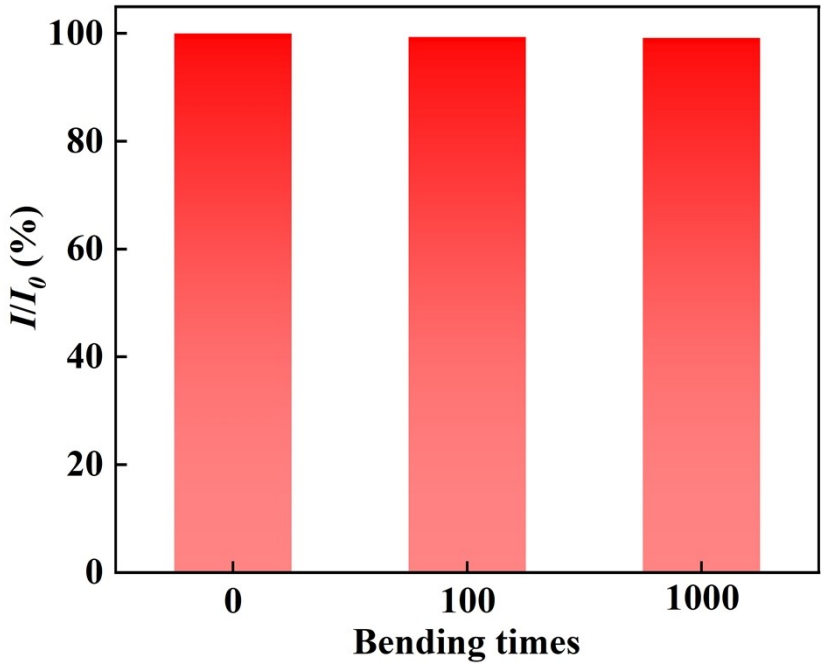

Figure S13 The rate of catalytic current change in the CNT-bioanode after 100 and 1000 bends.

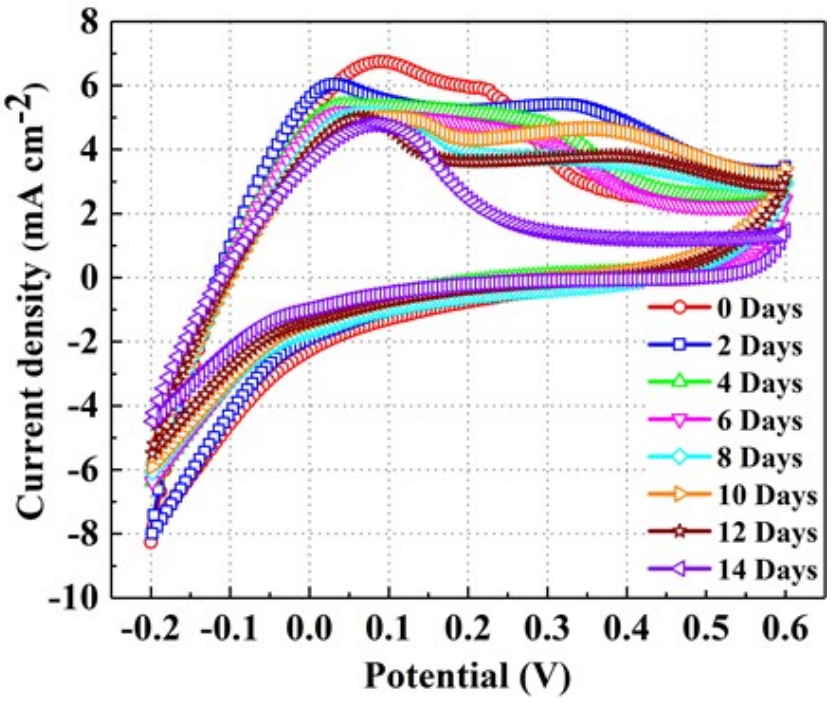

Figure S14 The CV curves of CNT-bioanode at different life cycles.

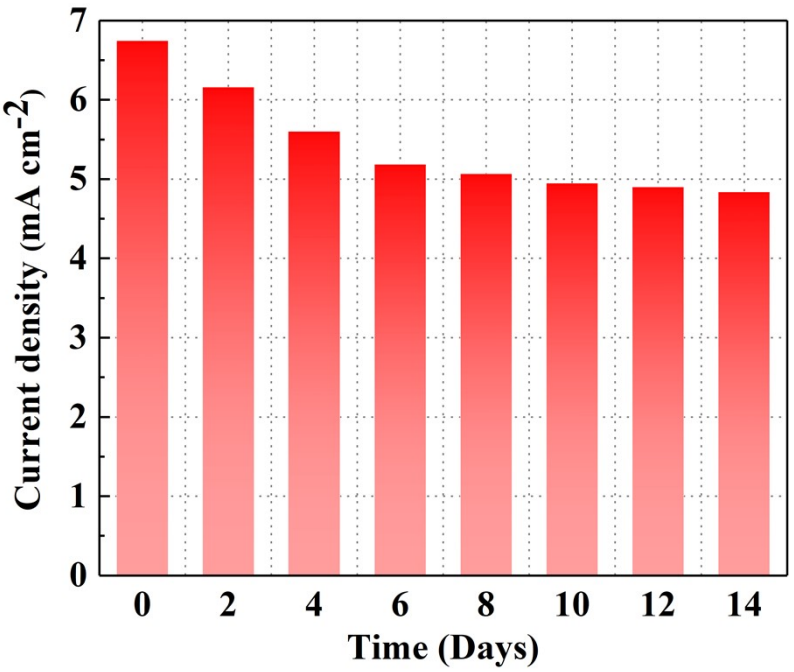

Figure S15 Maximum catalytic current of CNT-bioanodes at different life cycles.

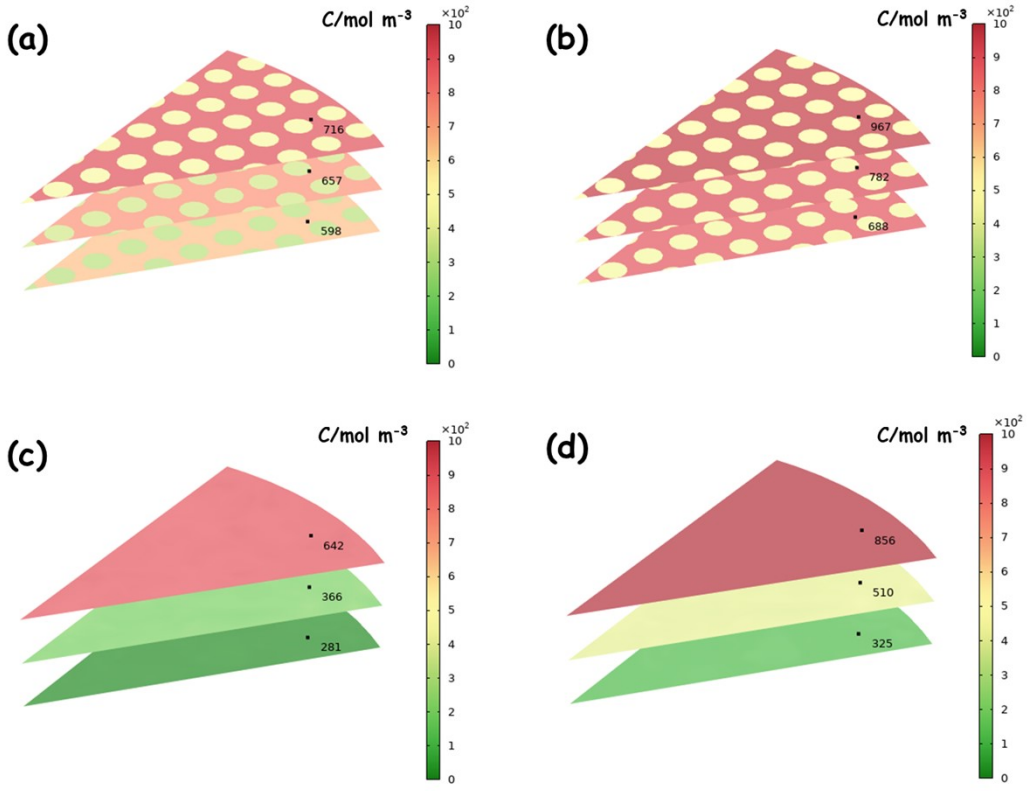

Figure S16 Lactate concentration distribution in the CNT-bioanode for before (a and b) and (c and d) after the elimination of a hierarchical porous structure at the initial 10min (a and c) and the end 60 min (b and d).

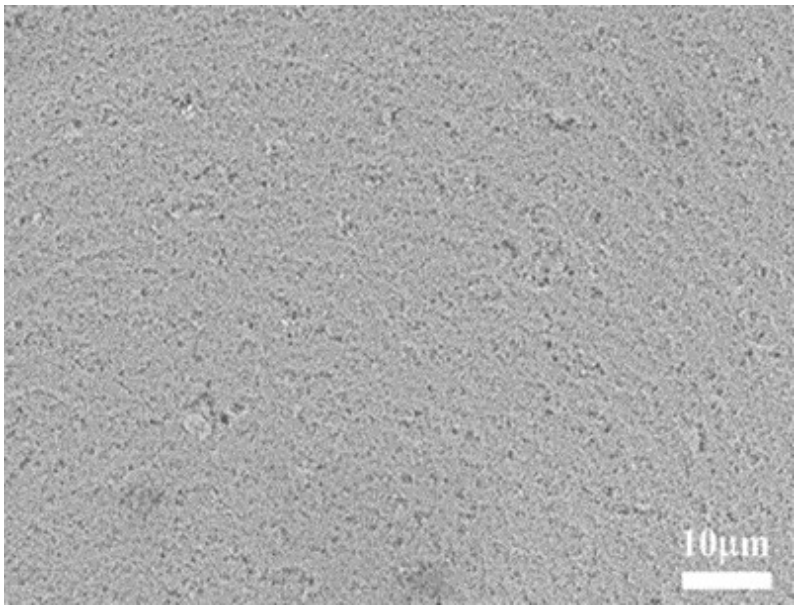

Figure S17 The SEM image of Pt/C on the surface of the hydrophobic carbon cloth.

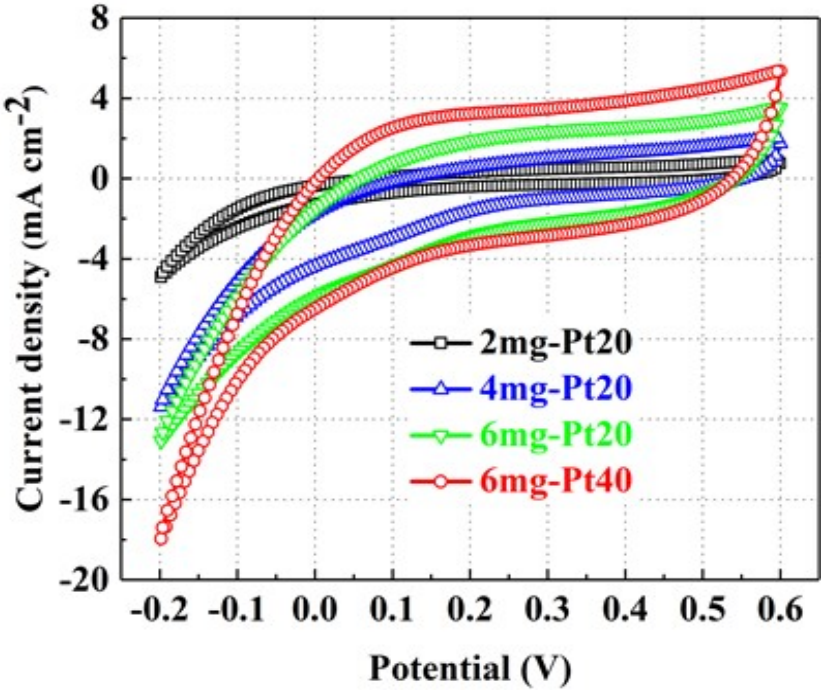

Figure S18 The CV curves of the different Pt content of air-cathode.

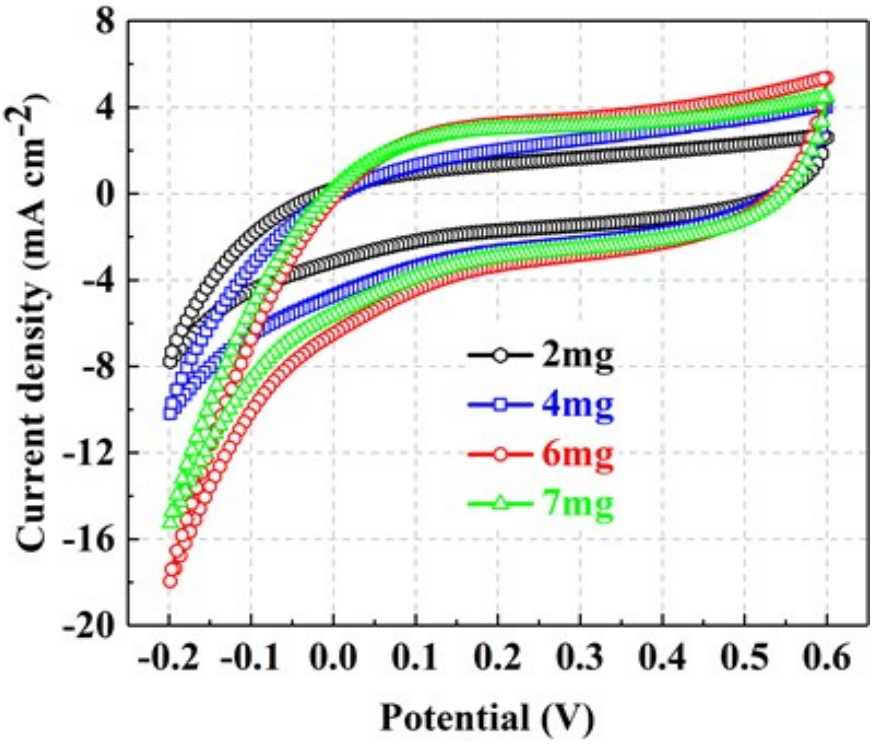

Figure S19 The CV curves of different catalyst loads of air-cathode.

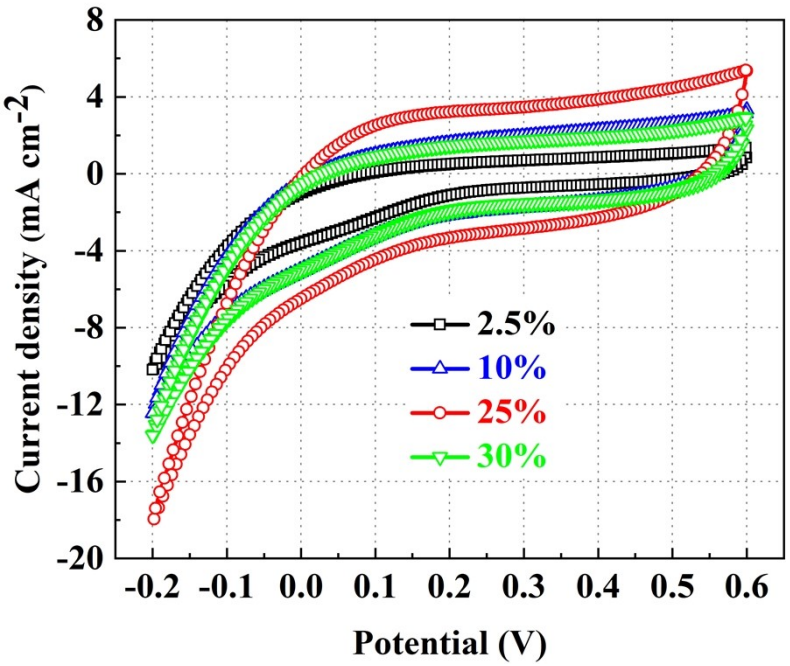

Figure S20 The CV curves of different Nafion loads of air-cathode.

Supplementary Note 2

The hydrophilic/hydrophobic design of the interface played a crucial role in regulating the three-phase boundary. Figure S18-S20 visually explored the design process of three-phase interface based on the reduction current. In details, the maximum reduction current increased progressively with an increase in Pt content from 20 % to 40 %, reaching a peak value of 18.1 mA/cm^2, which was significantly higher than the initial value of 4.9 mA/cm^2 (Figure S18). And the maximum reduction current exhibited a peak value at 6 mg of 40 % Pt content (Figure S19). The weight increase of the Pt/C catalyst resulted in a certain surface thickness, which elevated the resistance to O_2 transport and consequently lead to a decrease in the reduction current. Besides, the excessive hydrophilicity of the three-phase interface would inevitably lead to an increase in oxygen transmission resistance. The optimal amount of Nafion was observed at 25 % (Figure S20).

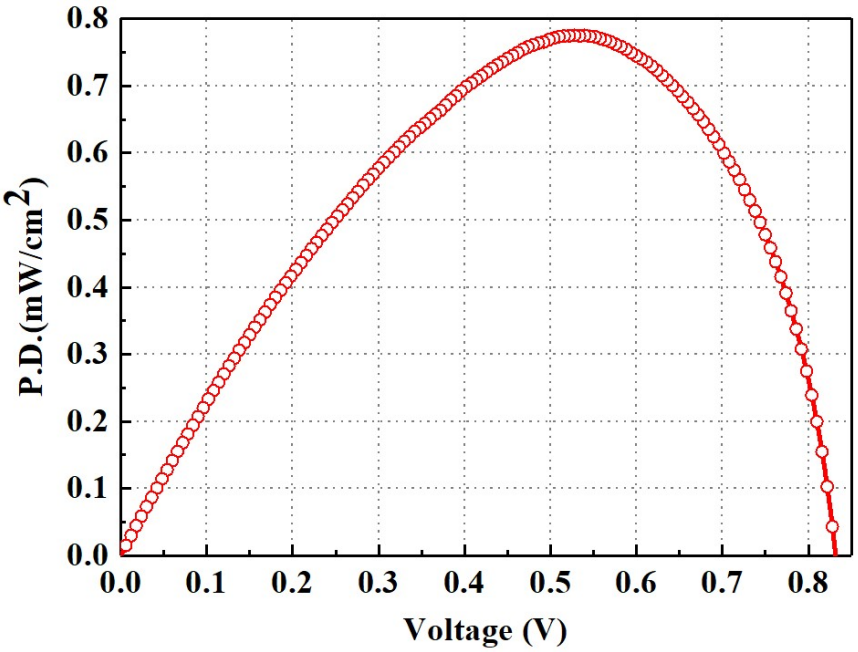

Figure S21 The output power density curves of the CNT-bioanode after eliminating the porous structure on BFCs.

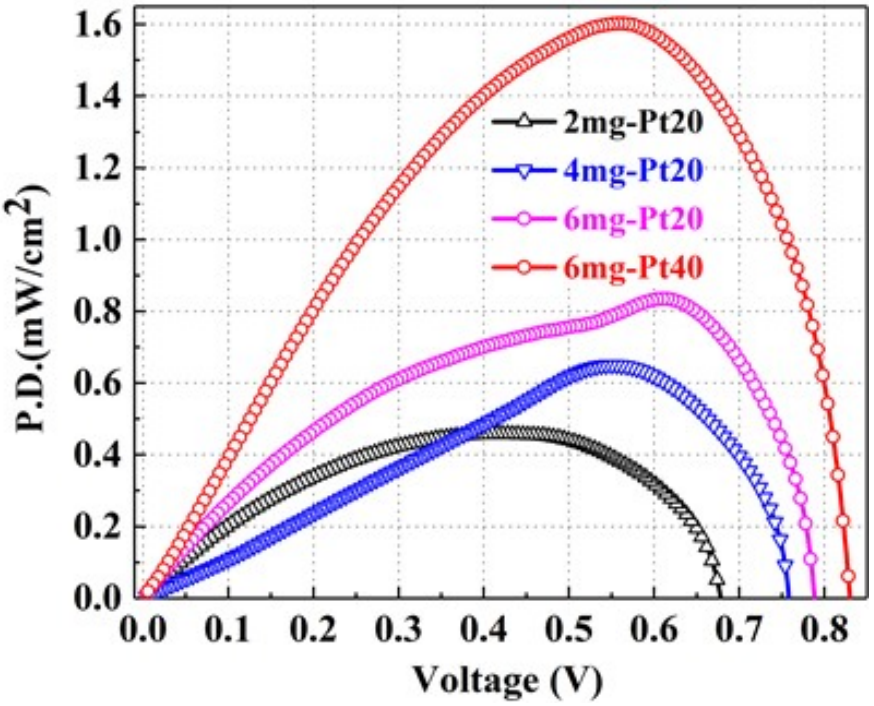

Figure S22 The output power density curves of the different air-cathode with Pt content on BFCs.

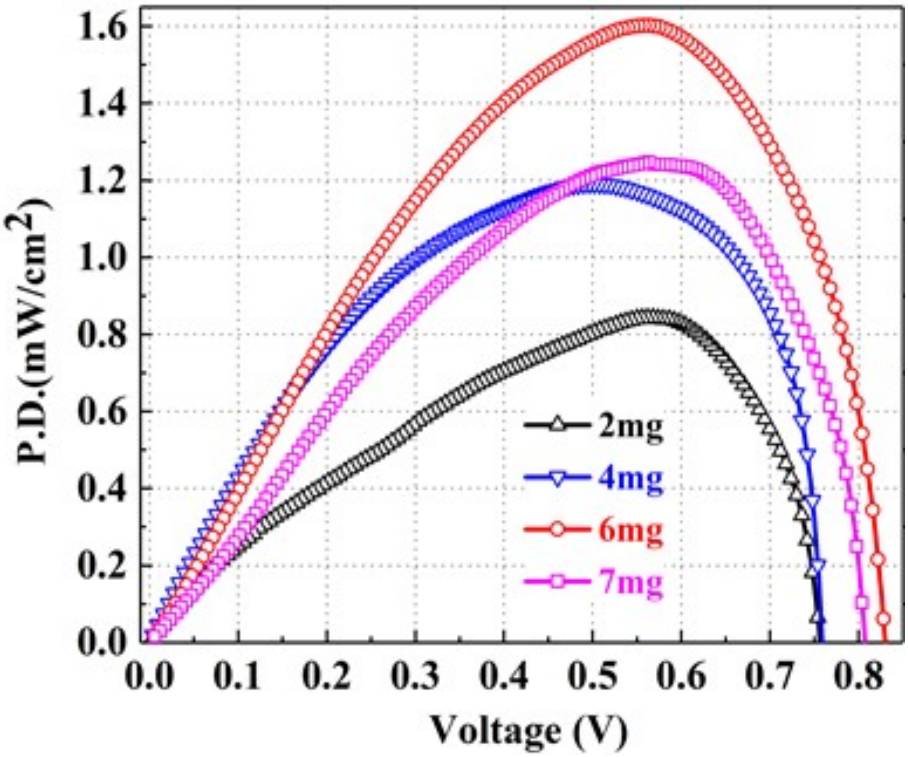

Figure S23 The output power density curves of the different air-cathode with catalyst content on BFCs.

Supplementary Note 3

Figure S22 and S23 demonstrated that a well-designed three-phase interface was also an essential prerequisite for fully exploiting the electrochemical performance of CNT-bioanodes. Therefore, we can conclude that the excellent power density of BFCs was primarily attributed to the synergistic effect of the hierarchical pore structure of CNT-bioanode and superior three-phase interface of air-cathode.

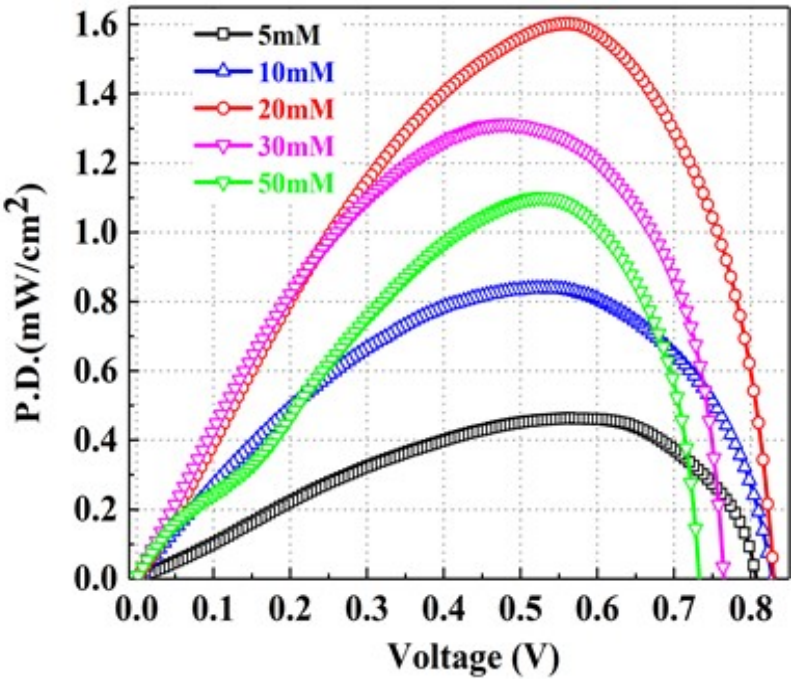

Figure S24 The output power density curves of the BFCs in different artificial sweat.

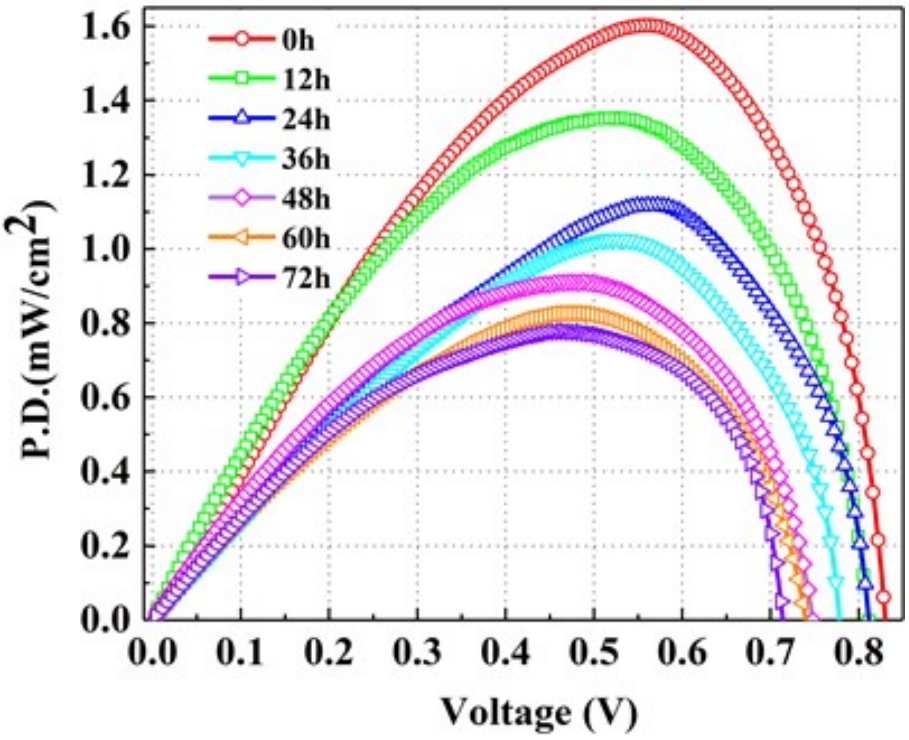

Figure S25 The output power density curves of the BFCs in 72 hours.

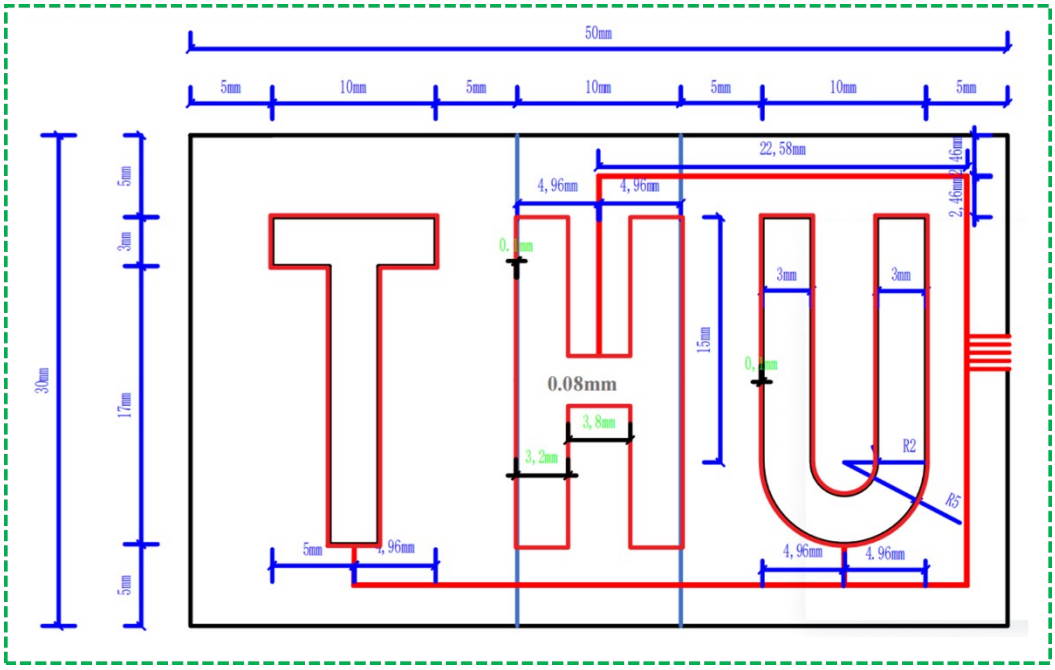

Figure S26 Schematic diagram of a conductive module for electron transfer.

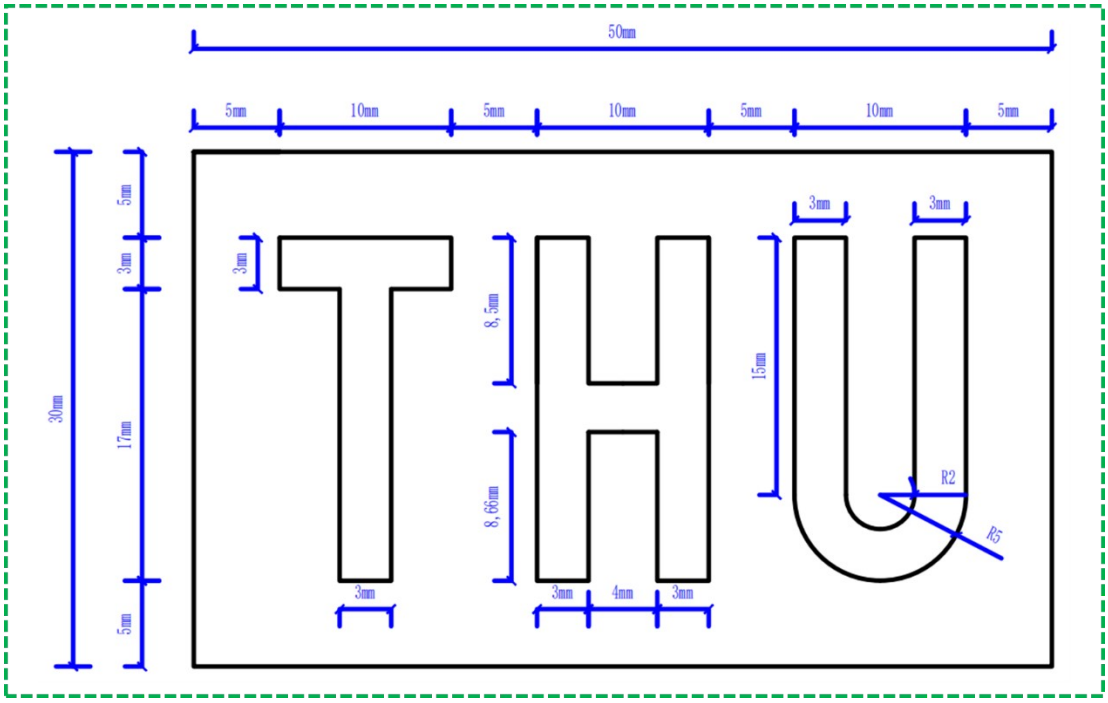

Figure S27 Schematic diagram of the reaction chamber module construction of the "THU" shaped structure.

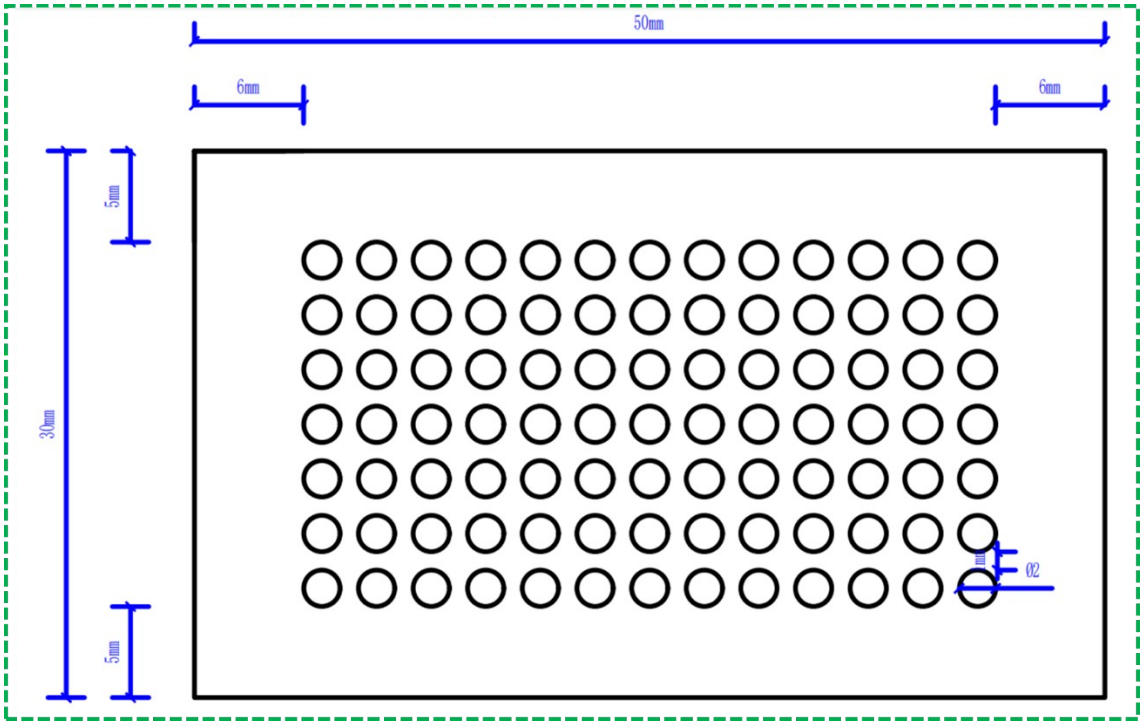

Figure S28 Schematic diagram of the microchannel module attached to the skin interface.

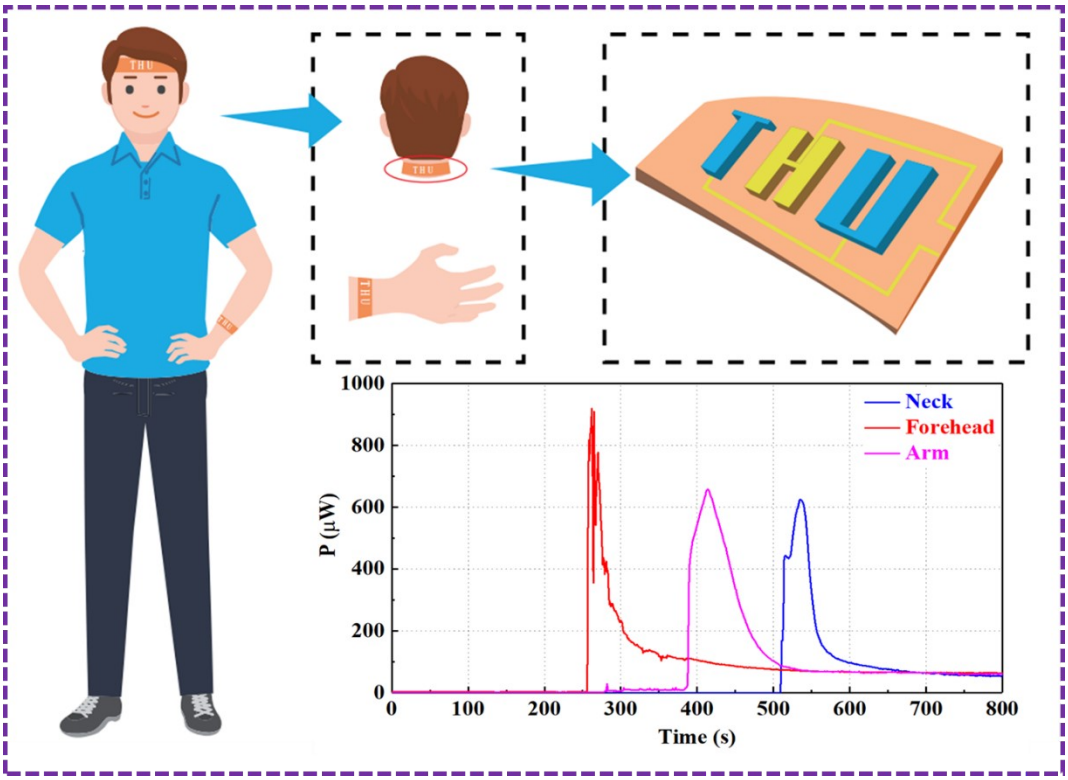

Figure S29 The schematic diagram of the HSBFC conformal with the human body and the energy curve generated by the sweat of the volunteers during exercise displayed in real time at the corresponding position.

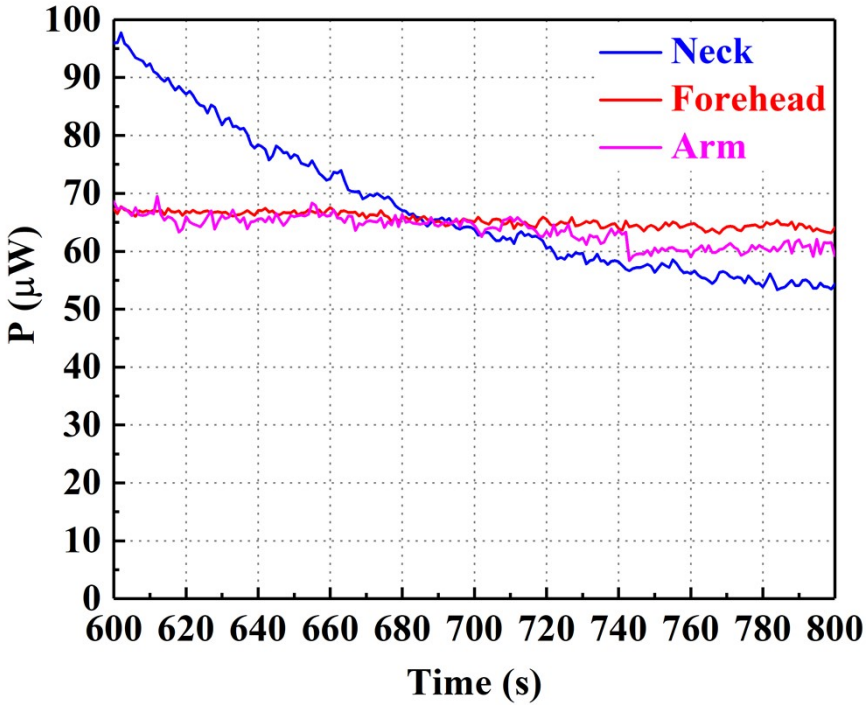

Figure S30 Schematic diagram of HSBFC maintaining energy output in the epidermal sweat environment of volunteers.

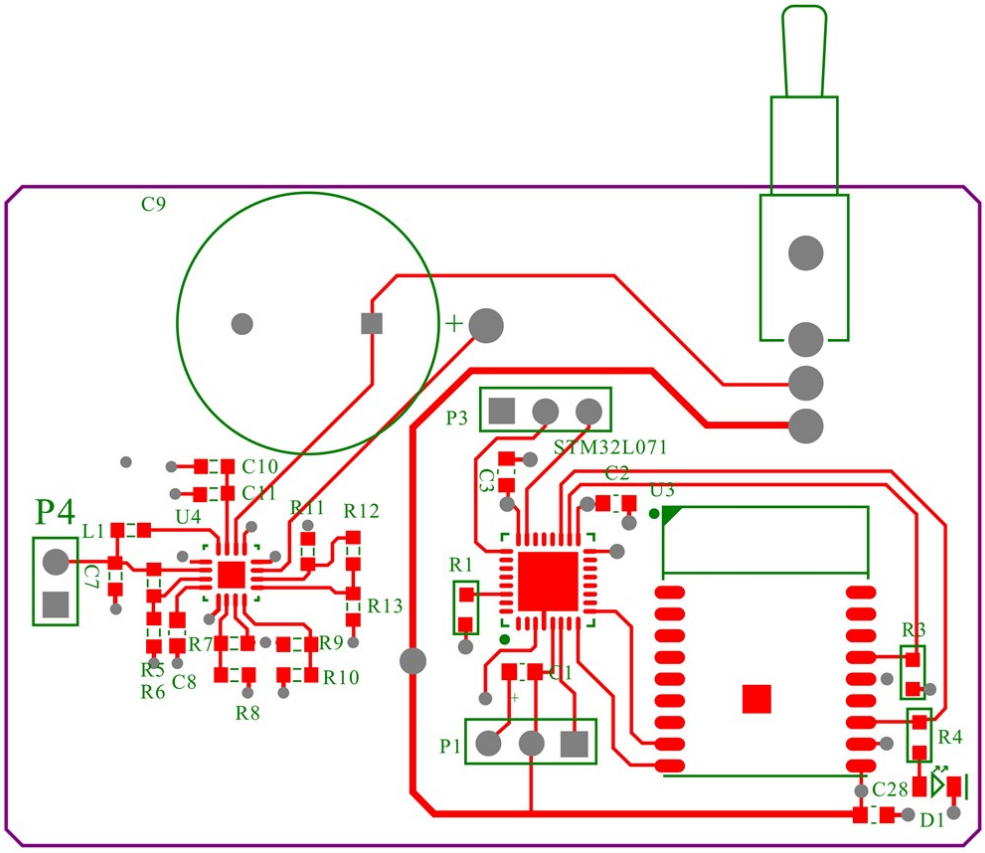

Figure S31 Schematic design of integrated circuits.

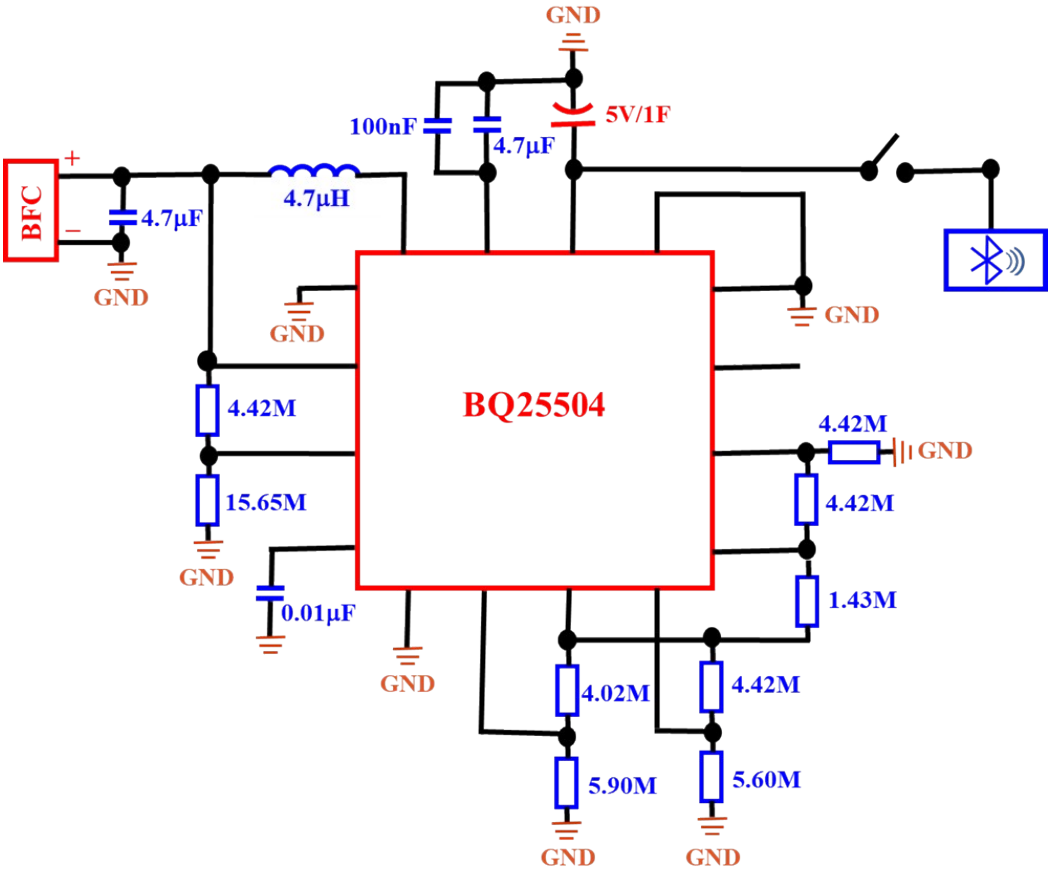

Figure S32 Schematic design of BQ25504.

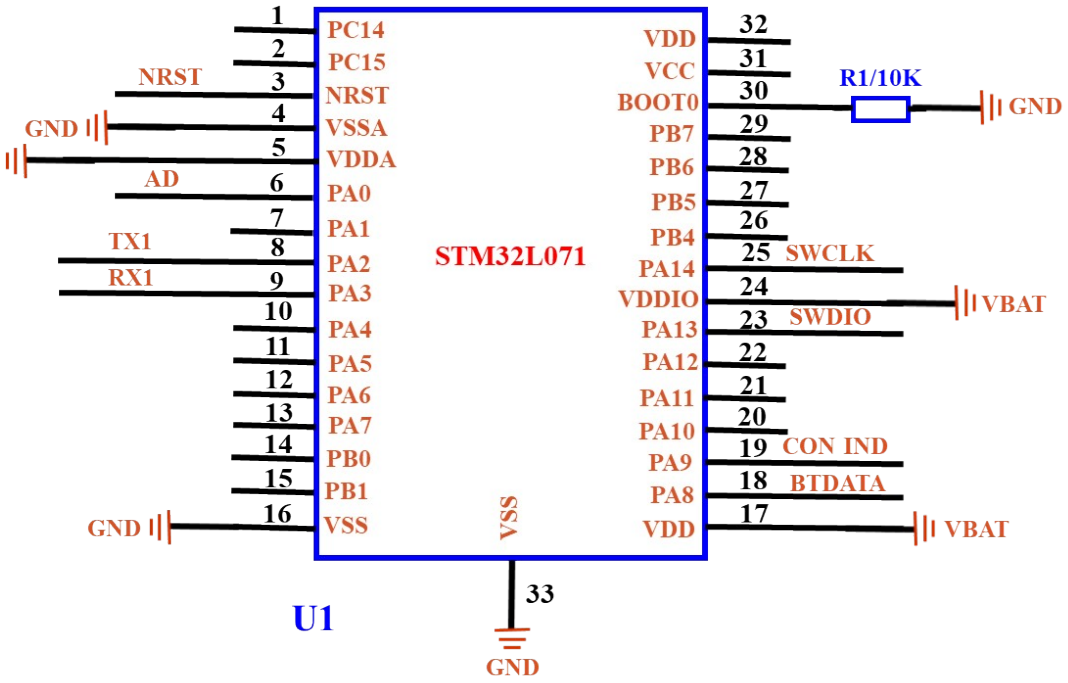

Figure S33 Schematic design of CPU.

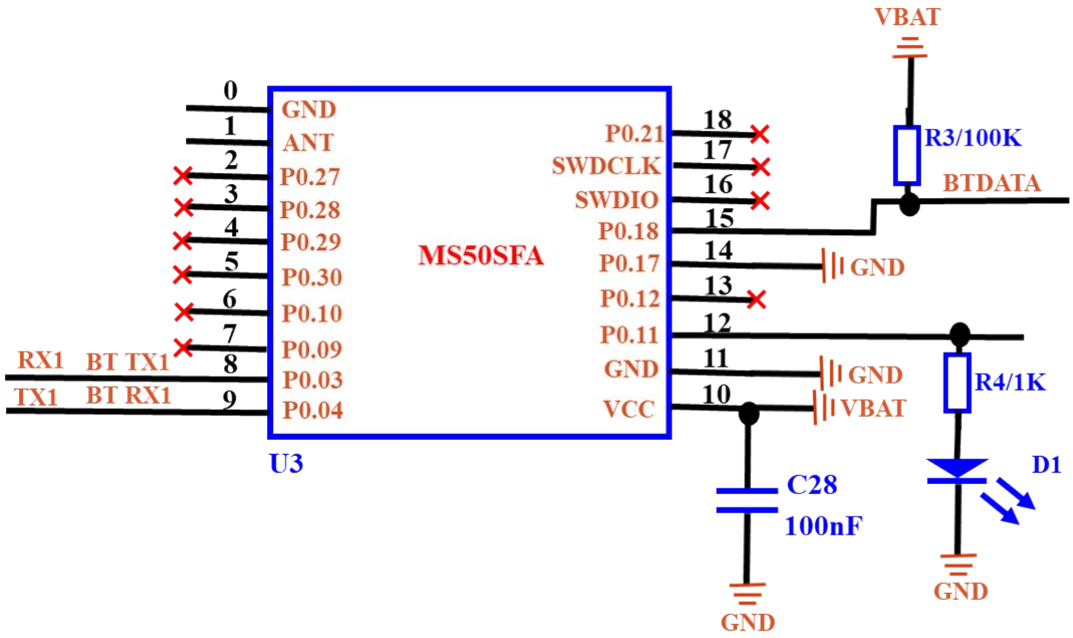

Figure S34 Schematic design of Bluetooth.

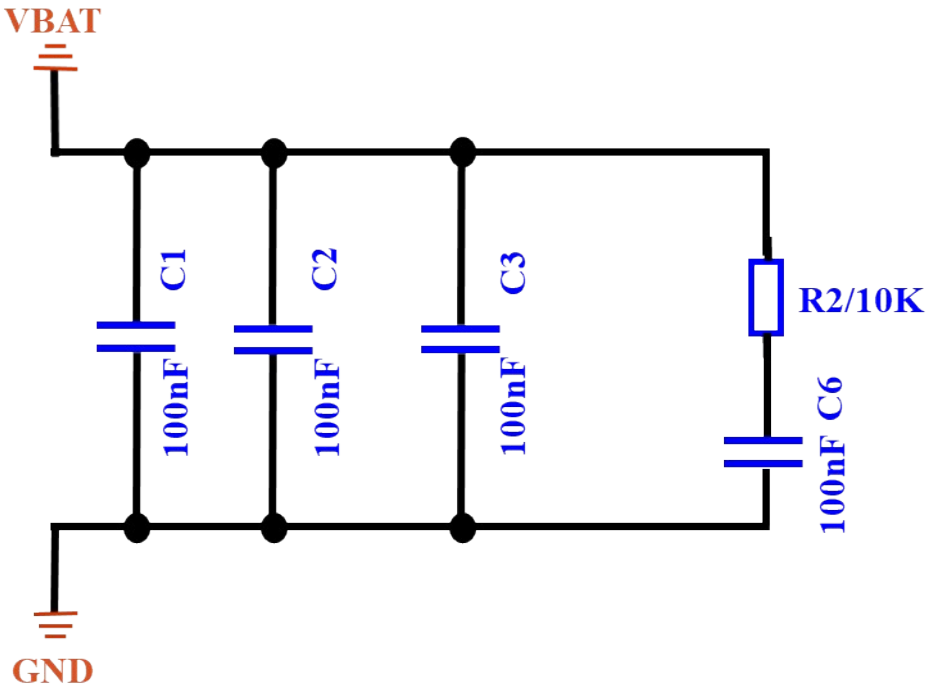

Figure S35 Schematic design of CPU coupled circuits.

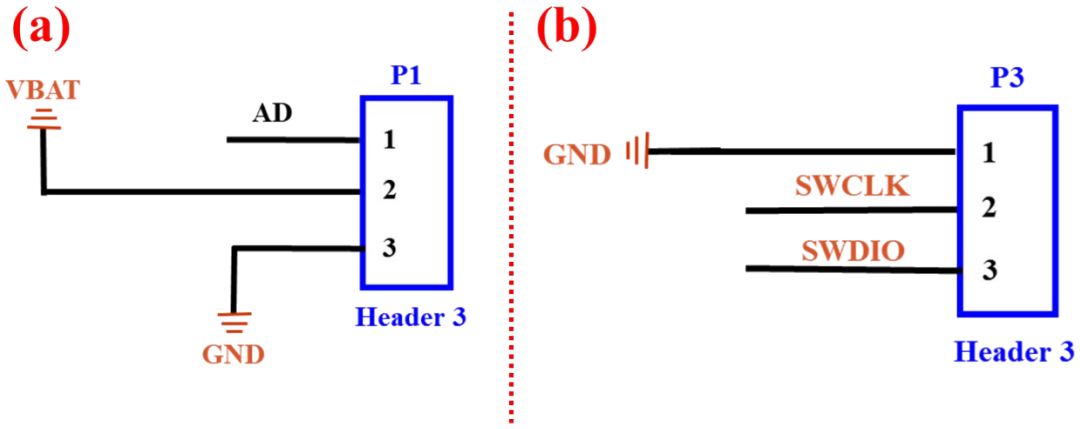

Figure S36 Schematic design of coupled circuits on integrated circuits.

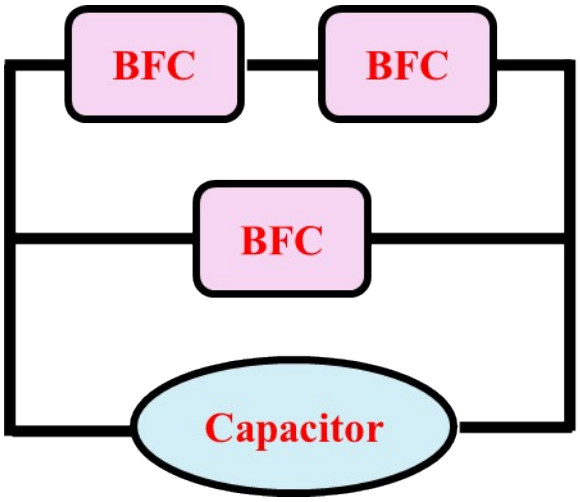

Figure S37 Three BFCs can charge the capacitor to 1F within approximately 40min.